

A FRET operated sensor for intracellular pH mapping: strategically improved efficiency on moving from an anthracene to a naphthalene derivative†

Cite this: *RSC Advances*, 2013, **3**, 14397

Arnab Banerjee,^a Animesh Sahana,^a Sisir Lohar,^a Bidisha Sarkar,^b Subhra Kanti Mukhopadhyay^b and Debasis Das^{*a}

Received 3rd April 2013
Accepted 31st May 2013

DOI: 10.1039/c3ra41591k

www.rsc.org/advances

Two novel fluorescent probes based on anthracene (AAC) and naphthalene (ANC) have been synthesised and characterised. Both the AAC and ANC derivative show green fluorescence at basic pH, but at acidic pH AAC is non-fluorescent, while ANC emits red light. This is attributed primarily to the FRET on-off processes. ANC has better pH discrimination abilities than AAC and can be used to distinguish between different pH environments inside a living cell for the first time.

1. Introduction

Intracellular pH plays an important role^{1,2} in different physiological and pathological processes *viz.* cell growth and apoptosis,^{3,4} the proliferation of multidrug resistance (MDR),⁵ ion transport,^{6,7} calcium regulation and cell adhesion,⁸ endocytosis,⁴ along with homeostasis and muscle contraction.⁹ An unusual intracellular pH indicates irregular cell function, growth and division, and is commonly observed in cancers¹⁰ and Alzheimer's disease.¹¹ The acidic environment in lysosomes (pH 4.5–5.5)^{12,13} facilitates the degradation of proteins in cellular metabolism. Intracellular pH becomes alkaline (≥ 8.0)¹⁴ at the early stage of pollen grain germination. Therefore, pH responsive fluorescent probes with different colours at acidic and basic pH are in high demand for biological applications. Most of the reported fluorescent pH sensors function either in the acidic or basic range and have not been used for intracellular studies.¹⁵ Most importantly, they are not sensitive in the vicinity of neutral pH, and hence, not useful for monitoring intercellular pH. Noticeably, most previously reported pH sensors are polymers or large molecules that requires tedious and expensive synthetic protocols. Presently, we are working to develop an inexpensive small molecule/analyte for use as a selective fluorescent sensor.¹⁶

Selective determination of an analyte with a FRET based probe minimizes the effects of aggregation, photo bleaching or interference from accompanying biomolecules.¹⁷ One of the

best strategies for making an efficient FRET based pH sensor is that the wavelength of absorption of the acceptor varies with pH. The absorption wavelength of 2,6-diformyl-4-methylphenol changes with pH and its Schiff base contains an extended conjugation system making the *p*-cresol unit a good acceptor. Initially, we have chosen anthracene as a donor unit because its emission energy is comparable to the absorption energy of the *p*-cresol unit. On moving from the anthracene to a naphthalene derivative, the pH dependent FRET process can be tuned significantly resulting in a pH sensor that can operate at both acidic and basic pH.

The probe based on AAC contains three units, *viz.* 2-aminothiophenol, an anthracene compound, and *p*-cresol, whereas in the ANC probe, the anthracene is replaced by a naphthalene compound. Scheme 1 shows an outline of their synthesis.

2. Experimental

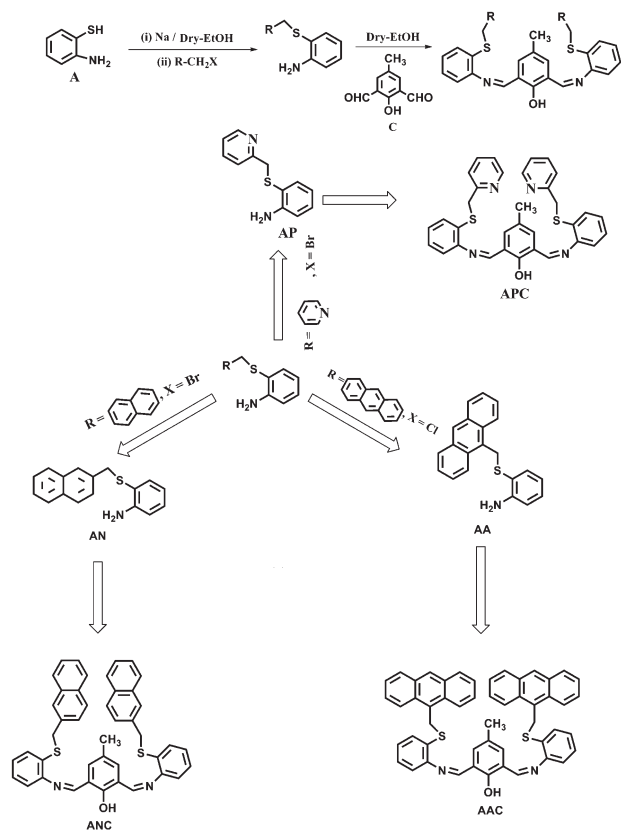
2.1 General procedures

2-Aminothiophenol, 9-chloromethyl anthracene and 2-bromomethyl naphthalene were purchased from Sigma-Aldrich (India). *p*-Cresol, *p*-formaldehyde and hexamethylenetetramine were purchased from Merck (India). Spectroscopic grade solvents were used. Other analytical reagent grade chemicals were used without further purification. Milli-Q 18.2 M Ω cm⁻¹ water was used throughout all of the experiments. A JASCO (model V-570) UV-Vis spectrophotometer was used for measuring the absorption spectra. FTIR spectra were recorded on a JASCO FTIR spectrometer (model: FTIR-H20). Mass spectra were obtained using a QTOF Micro YA 263 mass spectrometer in ES positive mode. ¹H NMR spectra were recorded using Bruker Advance 300 (300 MHz), 400 (400 MHz) and 500 (500 MHz) instruments in CDCl₃. ¹³C NMR spectra have been recorded using Bruker Advance 400 (100 MHz) and 500 (125 MHz) instruments in CDCl₃ or DMSO-d₆.

^aDepartment of Chemistry, The University of Burdwan, Burdwan-713104, West Bengal, India

^bDepartment of Microbiology, The University of Burdwan, Burdwan-713104, West Bengal, India. E-mail: ddas100in@yahoo.com; Fax: +91-342-2530452; Tel: +91-342-2533913

† Electronic supplementary information (ESI) available. See DOI: 10.1039/c3ra41591k



Scheme 1

Elemental analysis was performed using a Perkin Elmer CHN analyser with a first 2000 analysis kit. Steady-state fluorescence experiments were performed using a Hitachi F-4500 spectrofluorimeter. Time-resolved fluorescence life time measurements were carried out using a picosecond pulsed diode laser-based time-correlated single photon counting (TCSPC) spectrometer from IBH (UK) at 375 nm (λ_{ex}) with a MCP-PMT detector. The emission from the sample was collected at a right angle to the direction of the excitation beam maintaining a magic angle polarization of 54.71. The full width at half maximum (FWHM) of the instrument response function is 250 ps and the resolution is 28 ps per channel. The data were fitted to multi-exponential functions after deconvolution of the instrument response function using an iterative reconvolution technique with IBH DAS 6.2 data analysis software in which reduced χ^2 and weighted residuals serve as parameters of best fit.

pH measurements were carried out using a Systronics digital pH meter (model 335, India). All spectra were recorded at room temperature. The structures of the probes at acidic, basic and neutral pH were optimized using DFT/TDDFT techniques. Theoretical calculations were performed at the DFT/B3LYP level with a 6-31G basis set using the Gaussian 03 software package.¹⁸ The optimized geometry of the probes in three different forms were performed in the gas phase as this represents the solid state structure. However, the theoretical UV-Vis spectra were generated by a TDDFT method using the CPCM formalism,¹⁹

and methanol was used as the solvent. The conductor-like polarizable continuum model (CPCM) considers the dielectric effect of the solvent.

2.2 Imaging system

The imaging system was composed of an inverted fluorescence microscope (Leica DM 1000 LED), a digital compact camera (Leica DFC 420C), and an image processor (Leica Application Suite v3.3.0). The microscope is equipped with a 50 W mercury arc lamp and a UV filter.

2.3 Preparation of the cells

Pollen grains were obtained from the freshly collected mature buds of *Tecoma stans*, a common ornamental plant with a bright yellow flower, by crushing the stamens on a sterile Petri plate, then suspending them in normal saline solution. Debris was removed by filtration through a thin layer of non-absorbent cotton. The suspended pollen was collected by centrifugation at 5000 rpm for 5 min. The pollen pellet was then washed twice in normal saline solution and incubated in a DMSO-buffer solution containing the probes (50 μM) for 1 h at room temperature. After incubation, the products were washed again with normal saline solution and observed under a fluorescence microscope using a UV filter.

2.4 Cell viability studies

At first, the pollen grains were treated with 10% HgCl_2 solution to sterilize their surfaces. The treated pollen was washed three times with a pH 7.0 buffer. One set of pollen was incubated in a pollen germination medium (PGM: 0.01% H_3BO_3 , 0.07% $\text{CaCl}_2 \cdot 2\text{H}_2\text{O}$, 3.0% PEG-4000 and 20% sucrose)³ and acted as a control. Another set of pollen was incubated in the same medium, but also containing the probes (AAC or AN, at pH 7.0). This set of pollen was then incubated for up to three days at 30–35 °C.

The pollen germination was monitored from time to time under a light microscope. The *Tecoma stans* pollen treated with the probes exhibited more than 90% viability, in terms of germination, compared to the control set.

2.5 Synthesis of 2-((anthracen-9-yl)methylthio)benzenamine (AA) (Scheme 1)

276.0 mg (12.0 mmol) of Na (a little more than a stoichiometric amount) was added pinch-wise to dry ethanol (20 mL, 0 °C) under a nitrogen atmosphere with constant stirring, until complete dissolution occurred. A solution of 2-aminothiophenol (1 g, 7.98 mmol in 5 mL dry EtOH) was added to the above solution, while stirring, over 30 min followed by the pinch-wise addition of 2.51 g (7.98 mmol) of 9-chloromethylanthracene. Stirring was continued for another 4 h at 70 °C. After removing the solvent using a rotary evaporator, the crude product was subjected to column chromatography (hexanes : EtOAc = 95 : 5, v/v). Yield, 90%. ¹H NMR (300 MHz, CDCl_3) (Fig. S1, ESI[†]): δ (ppm): 4.3 (2H, s); 4.9 (2H, s); 6.6 (1H, m, $J = 7.5$ Hz); 6.7 (1H, m, $J = 6.8$ Hz); 7.1 (1H, m, $J = 7.9$ Hz); 7.2 (1H, s); 7.3 (2H, m, $J = 6.18$ Hz); 7.5 (3H, m, $J = 3.3$ Hz); 8.0 (2H, m, $J = 4.4$ Hz); 8.2 (2H, m, $J = 7.3$ Hz); 8.3 (1H, m, $J = 5.1$ Hz). ¹³C

NMR (125 MHz, CDCl₃) (Fig. S2 and S3, ESI[†]): δ (ppm): 148.6, 136.8, 133.2, 132.4, 130.1, 128.1, 127.7, 127.6, 127.4, 127.1, 126.0, 125.7, 118.5, 114.9, 40.01. QTOF-MS ES⁺: [M + H]⁺ (Fig. S4, ESI[†]) = 316.4 (100%). Elemental analysis data calculated for C₁₇H₁₅NS (%): C, 76.94; H, 5.70 and N 5.28. Found (%): C, 77.43; H, 5.96 and N, 4.89.

2.6 Synthesis of 2,6-bis(-2-((anthracen-9-yl)methylthio)phenylimino)methyl)-4-methylphenol (AAC) (Scheme 1)

2,6-Diformyl-4-methylphenol was synthesized starting from *p*-cresol following a published procedure.²⁰ To a solution of 2,6-diformyl-4-methylphenol (0.328 g, 2 mmol in 20 mL dry methanol), AA (1.26 g, 4 mmol in 20 mL dry methanol) was added drop-wise while stirring. The reaction mixture was refluxed for 4 h. After removing the solvent using a rotary evaporator, the crude product was purified by column chromatography (hexanes : EtOAc = 82 : 18, v/v). Yield, 75%. M. P. = 130 °C (\pm 1 °C). ¹H NMR (300 MHz, CDCl₃) (Fig. S5, ESI[†]): δ (ppm): 2.1 (3H, s); 4.2 (4H, m, *J* = 7.8 Hz); 7.4–7.1 (8H, m, *J* = 8.1 Hz); 7.8 (2H, t, *J* = 13.5 Hz); 8.2–8.0 (14H, m, *J* = 8.7 Hz); 8.5 (2H, d, *J* = 8.2 Hz); 8.7 (2H, d, *J* = 9.4 Hz); 9.3 (2H, s); 13.7 (1H, d, *J* = 8.2 Hz); ¹³C NMR (125 MHz, CDCl₃) (Fig. S6 and S7, ESI[†]): δ (ppm): 163.1; 143.3; 137.3; 135.8; 134.0; 131.8; 131.5; 131.2; 130.1; 129.2; 129.1; 127.9; 127.5; 126.7; 125.9; 125.5; 125.23; 125.0; 124.6; 59.9; 40.1. QTOF-MS ES⁺: [M + H]⁺ (Fig. S8, ESI[†]) = 759.25 (100%). Elemental analysis data calculated for C₄₃H₃₄N₂OS₂(%): C, 78.39; H, 5.20; N, 4.25. Found (%): C, 78.84; H, 4.79; N, 4.82. No monomer has been found.

2.7 Synthesis of 2-((naphthalen-6-yl)methylthio)benzenamine (AN) (Scheme 1)

276.0 mg (12.0 mmol) of Na was added pinch-wise to 20 mL of dry EtOH under a nitrogen atmosphere (at 0 °C) with constant stirring, until complete dissolution occurred. A 5 mL solution of 2-aminothiophenol (1 g, 7.98 mmol in dry EtOH) was then added, while stirring, over 30 min followed by the addition of 1.76 g (7.98 mmol) of 2-bromomethylnaphthalene. Stirring was continued for another 2 h. After removing the solvent using a rotary evaporator, the crude product was subjected to column chromatography (hexanes : EtOAc = 95 : 5, v/v). Yield, 85%. ¹H NMR (300 MHz, CDCl₃) (Fig. S9, ESI[†]): δ (ppm): 4.0 (2H, s); 4.2 (2H, s); 6.5 (1H, t, *J* = 7.2 Hz); 6.6 (1H, d, *J* = 7.5 Hz); 7.1 (1H, t, *J* = 7.8 Hz); 7.2 (1H, m, *J* = 0.9 Hz); 7.3 (1H, m, *J* = 1.5 Hz); 7.4 (3H, m, *J* = 3.3 Hz); 7.7 (1H, m, *J* = 3.3 Hz); 7.9 (2H, m, *J* = 4.5 Hz); ¹³C NMR (125 MHz, CDCl₃) (Fig. S10, ESI[†]) 148.7; 136.6; 131.5; 130.3; 130.0; 129.0; 127.4; 125.9; 125.0; 124.1; 118.6; 114.8; 32.5. QTOF-MS ES⁺: [M + H]⁺ (Fig. S11, ESI[†]) = 266.01 (100%). Elemental analysis data calculated for C₁₇H₁₅NS (%): C, 76.94; H, 5.70 and N, 5.28. Found (%): C, 77.23; H, 5.86 and N, 4.99.

2.8 Synthesis of 2-(-2-((naphthalen-2-yl)methylthio)phenylimino)methyl)-6-(2-((naphthalen-3-yl)methylthio)phenylimino)methyl)-4-methylphenol (ANC) (Scheme 1)

To a solution of 2,6-diformyl-4-methylphenol (0.328 g, 2 mmol in 30 mL methanol), AN (1.06 g, 4 mmol in 20 mL methanol) was added drop-wise while stirring. The reaction mixture was

refluxed for 4 h. After removing the solvent using a rotary evaporator, the crude product was purified by column chromatography (hexanes : EtOAc = 82 : 18, v/v). Yield, 75%. M. P. = 130 °C (\pm 1 °C). ¹H NMR (300 MHz, CDCl₃) (Fig. S12, ESI[†]): δ (ppm): 2.3 (3H, s); 4.2 (4H, s); 7.0 (4H, m, *J* = 7.2 Hz); 7.2 (6H, m, *J* = 7.5 Hz); 7.4 (8H, m, *J* = 5.1 Hz); 7.7 (8H, m, *J* = 7.5 Hz); ¹³C NMR (125 MHz, CDCl₃) (Fig. S13 and S14, ESI[†]) 159.6; 134.6; 133.3; 132.3; 132.5; 131.8; 128.2; 127.7; 127.6; 127.5; 127.3; 127.1; 127.0; 126.1; 125.7; 118.1; 117.9; 40.0; 20.3. QTOF-MS ES⁺ (Fig. S15 in ESI[†]): [M + H]⁺ = 659.23 (100%). Elemental analysis data calculated for C₄₃H₃₄N₂OS₂ (%): C, 78.39; H, 5.20 and N, 4.25. Found (%): C, 78.54; H, 4.89 and N, 4.52. The light yellow solid monomer was also formed in an 8% yield.

2.9 Synthesis of 2-((pyridin-2-yl)methylthio)benzenamine (AP) (Scheme 1)

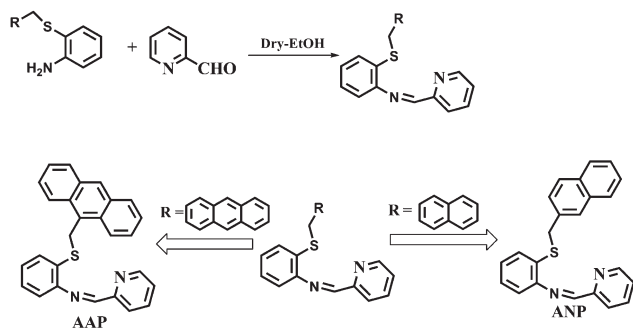
276.0 mg (12.0 mmol) of Na was added pinch-wise to 20 mL of dry EtOH under a nitrogen atmosphere (at 0 °C) with constant stirring, until complete dissolution occurred. A 5 mL solution of 2-aminothiophenol (1 g, 7.98 mmol in dry EtOH) was then added, while stirring, over 30 min followed by the addition of 2.02 g (7.98 mmol) of 2-bromomethylpyridine hydrobromide. Stirring was continued for another 2 h. After removing the solvent using a rotary evaporator, the crude product was subjected to column chromatography (hexanes : EtOAc = 95 : 5, v/v). Yield, 80%. ¹H NMR (400 MHz, CDCl₃) (Fig. S16, ESI[†]): δ (ppm): 3.9 (2H, s); 3.9 (2H, s); 6.5 (1H, t, *J* = 7.6 Hz); 6.6 (1H, d, *J* = 8 Hz); 6.9 (1H, d, *J* = 7.6 Hz); 7.0 (2H, m, *J* = 5.2 Hz); 7.1 (1H, d, *J* = 8 Hz); 7.4 (1H, m, *J* = 7.6 Hz); 8.4 (1H, d, *J* = 4.4 Hz). QTOF-MS ES⁺: [M + H]⁺ (Fig. S17, ESI[†]) = 217.17 (100%). Elemental analysis data calculated for C₁₂H₁₂N₂S (%): C, 66.63; H, 5.59 and N, 12.95. Found (%): C, 66.46; H, 5.63 and N, 13.04.

2.10 Synthesis of 2,6-bis((Z)-2-((pyridin-2-yl)methylthio)phenylimino)methyl)-4-methylphenol (APC) (Scheme 1)

To a solution of 2,6-diformyl-4-methylphenol (0.328 g, 2 mmol in 30 mL methanol), AP (0.864 g, 2 mmol in 20 mL methanol) was added drop-wise while stirring. The reaction mixture was refluxed for 4 h. After removing the solvent using a rotary evaporator, the crude product was purified by column chromatography (hexanes : EtOAc = 82 : 18, v/v). Yield, 65%. ¹H NMR (400 MHz, CDCl₃) (Fig. S18, ESI[†]): δ (ppm): 2.3 (3H, s); 3.9 (4H, s); 6.5 (3H, m, *J* = 7.6 Hz); 7.2 (10H, m, *J* = 6.8 Hz); 7.4 (5H, m, *J* = 7.6 Hz); 8.5 (2H, m, *J* = 4.4 Hz); 8.8 (2H, s); 10.4 (1H, s); ¹³C NMR (100 MHz, CDCl₃) (Fig. S19, ESI[†]) 163.5; 158.9; 157.2; 155.5; 149.0; 136.8; 132.5; 129.4; 128.03; 127.4; 127.1; 126.6; 126.1; 123.3; 122.2; 118.1; 114.3; 37.1; 20.0. QTOF-MS ES⁺ (Fig. S20, ESI[†]): [M + H]⁺ = 561.1 (100%). Elemental analysis data calculated for C₃₃H₂₈N₄OS₂ (%): C, 70.68; H, 5.03 and N, 9.99. Found (%): C, 70.54; H, 4.99 and N, 10.07. No monomer was detected.

2.11 Synthesis of (Z)-2-((anthracen-9-yl)methylthio)-N-((pyridin-2-yl)methylene)benzenamine (AAP) (Scheme 2)

To a solution of pyridine-2-carboxaldehyde (0.328 g, 2 mmol in 30 mL methanol), AA (0.864 g, 2 mmol in 20 mL methanol) was



Scheme 2

added drop-wise while stirring. The reaction mixture was refluxed for 4 h. After removing the solvent using a rotary evaporator, the crude product was purified by column chromatography (hexanes : EtOAc = 82 : 18, v/v). Yield, 65%. ^1H NMR (500 MHz, CDCl_3) (Fig. S21, ESI †): δ (ppm): 5.1 (2H, s); 7.1 (3H, m, $J = 10.0$ Hz); 7.3 (2H, m, $J = 2.5$ Hz); 7.4 (5H, m, $J = 4.5$ Hz); 7.9 (2H, m, $J = 6.5$ Hz); 8.1 (1H, m, $J = 7.5$ Hz); 8.3 (2H, d, $J = 9.0$ Hz); 8.3 (1H, s); 8.4 (1H, s); 8.5 (1H, d, $J = 4.0$ Hz); 8.6 (1H, d, $J = 4.0$ Hz). QTOF-MS ES $^+$ (Fig. S22, ESI †): $[\text{M} + \text{Na}]^+ = 427.04$ (100%). Elemental analysis data calculated for $\text{C}_{27}\text{H}_{20}\text{N}_2\text{S}$ (%): C, 80.17; H, 4.98 and N, 6.92. Found (%): C, 80.34; H, 4.99 and N, 6.77.

2.12 Synthesis of (Z)-2-(naphthalen-2-ylmethylthio)-N-(pyridin-2-ylmethylene)aniline (ANP) (Scheme 2)

To a solution of pyridine-2-carboxaldehyde (0.328 g, 2 mmol in 30 mL methanol), AN (0.864 g, 2 mmol in 20 mL methanol) was added drop-wise with stirring. The reaction mixture was refluxed for 4 h. After removing the solvent using a rotary evaporator, the crude product was purified by column chromatography (hexanes : EtOAc = 82 : 18, v/v). Yield, 65%. M. P. = 125 $^\circ\text{C}$ (± 1 $^\circ\text{C}$). ^1H NMR (500 MHz, CDCl_3) (Fig. S23, ESI †): δ (ppm): 4.3 (2H, s); 7.0 (1H, m, $J = 7.6$ Hz); 7.2 (2H, m, $J = 7.0$ Hz); 7.3 (1H, m, $J = 4.5$ Hz); 7.4 (2H, m, $J = 5.0$ Hz); 7.5 (1H, m, $J = 8.5$ Hz); 7.8 (6H, m, $J = 6.5$ Hz); 8.3 (1H, d, $J = 8.0$ Hz); 8.5 (1H, s); 8.6 (1H, d, $J = 4.5$ Hz). QTOF-MS ES $^+$ (Fig. S24, ESI †): $[\text{M} + \text{Na}]^+ = 377.01$ (100%). Elemental analysis data calculated for $\text{C}_{33}\text{H}_{28}\text{N}_4\text{OS}_2$ (%): C, 77.93; H, 5.12 and N, 7.90. Found (%): C, 77.84; H, 4.99 and N, 8.07.

3. Results and discussion

3.1 Absorption studies

The effect of pH on the UV-Vis spectra of AAC and ANC (in methanol-water, 7 : 3, v/v) is presented in Fig. S25 and S26 (ESI †), respectively. Methanol is chosen instead of a buffer as the solvent in order to compare the results with the theoretical TDDFT studies. At low pH, AAC shows three peaks at 355.0, 375.0 and 395.0 nm, which can be attributed to the anthracene unit (Fig. S25, ESI †). With a gradual increase in the pH, a new peak at 439.0 nm appears (at pH 7.0), the absorbance of which gradually increases with increasing pH, which is coupled with a concomitant decrease in the absorbance at 355.0, 375.0 and

395.0 nm, respectively. This new peak at 439.0 nm is attributed to the phenolate ion, which is also supported by the theoretical TDDFT results (*vide infra*).

In the case of ANC, an increase of pH (above pH 7.0) causes a decrease in the absorbance at 365 nm, with a concomitant increase at 437 nm through an isobestic point at 398 nm (Fig. S26, ESI †). In acidic pH, the peak at 365 nm undergoes a 25 nm blue shift to 340 nm and the absorbance of this peak increases with decreasing pH. Moreover, at acidic pH, a weak intra-molecular charge transfer (ICT) from the naphthalene moiety to the AC unit (which is supported TDDFT studies *vide infra*) was observed at 525 nm. Interestingly, such a CT band is absent in the AAC example, probably due to the greater steric crowding of the anthracene moiety compared to naphthalene.

Thus, AAC is intense green at basic pH, faint yellow at neutral pH and colorless at acidic pH (inset, Fig. S24, ESI †). On the other hand, ANC is light green at basic pH, colorless at neutral pH and red at acidic pH (inset, Fig. S26, ESI †).

3.2 Emission studies

Fig. S27 in the ESI † shows that the excitation of AAC at 380 nm (in a DMSO-Britton-Robinson buffer, 1 : 9, v/v, pH 7.0) results in a very weak emission band at 460 nm (the donor emission of an AA unit) along with a strong emission band at 537 nm (the acceptor emission). At pH 5.0, the weak emission at 460 nm is enhanced, while the acceptor emission at 537 nm is suppressed (FRET OFF). The reverse phenomenon was observed at basic pH (pH 11.0, FRET ON). This is well supported by the fluorescence life time data. The emission intensity of AAC at 537 nm (in a DMSO-Britton-Robinson buffer, 1 : 9, v/v, $\lambda_{\text{ex}} = 450$ nm) increases from neutral (quantum yield = 0.31) to basic pH, whereas it decreases at acidic pH (pH 5.0, quantum yield = 0.14). Over pH 11.0 (quantum yield = 0.75) the emission intensity remains unaltered (Fig. 1(i)). The absorption peak of the C unit in AAC undergoes a blue shift at acidic pH, whereas the peak position remains the same both at neutral and basic pH. Thus, at basic and neutral pH, the emission spectrum of the AA unit overlaps with the absorption spectrum of the C unit resulting in FRET ON (Fig. 2a). However, FRET alone is not responsible for the fluorescence enhancement of AAC at basic pH, the strong extended delocalization of the lone pair of the phenoxide ion (Fig. 3a) 21 (which is greatly reduced at neutral pH) also has a significant contribution. In contrast, at acidic pH, both of the imine nitrogens get protonated, thus inhibiting the extended delocalization.

Replacement of the anthracene moieties by naphthalene units (ANC) causes dramatic changes in the fluorescence properties (Fig. 1(ii)). The emission intensity increases on moving from neutral to basic pH ($\lambda_{\text{em}} = 535$ nm, $\lambda_{\text{ex}} = 365$ nm, quantum yield = 0.01 at pH 7.0). Above pH 11.0, the emission intensity remains unaltered (quantum yield = 0.39 at pH 11.0). Interestingly, the emission intensity also increases with a decrease in pH (from pH 6.5) ($\lambda_{\text{em}} = 600$ nm, quantum yield = 0.48 at pH 2.0). Thus, the probe can recognize all three conditions, *viz.* acidic, basic and neutral pH. Fig. 2b demonstrates that the emission spectrum of the AN unit overlaps with the

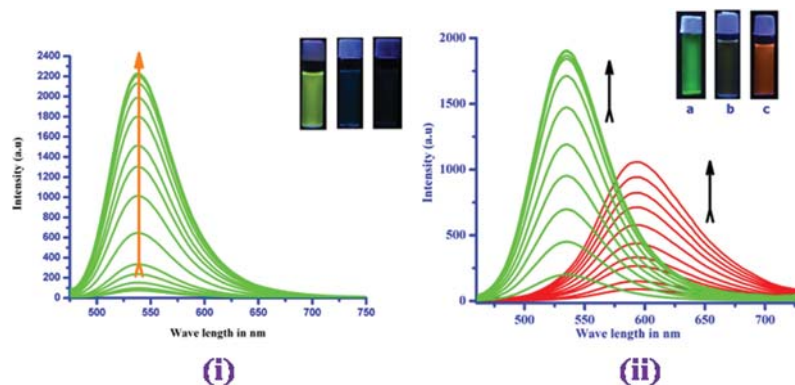


Fig. 1 Fluorescence spectra at different pH values: (i) AAC (10 μM) at pH (from bottom to top) 5.0, 5.5, 6.0, 6.5, 7.0, 7.5, 8.0, 8.5, 9.0, 9.5, 10.0, 10.5, 11.0 and 12.0. (ii) ANC (10 μM). Red lines (from bottom to top) indicate pH 6.5, 6.0, 5.5, 5.0, 4.5, 4.0, 3.5, 3.0, 2.5 and 2.0, whereas green lines (from bottom to top) indicate pH 7.0, 7.5, 8.0, 8.5, 9.0, 9.5, 10.0, 10.5, 11.0, 11.5 and 12.0. Inset: a, b and c show the colours at basic, neutral and acidic pH, respectively. (Solvent: DMSO–Britton–Robinson buffer, 1 : 9, v/v, $\lambda_{\text{ex}} = 450 \text{ nm}$).

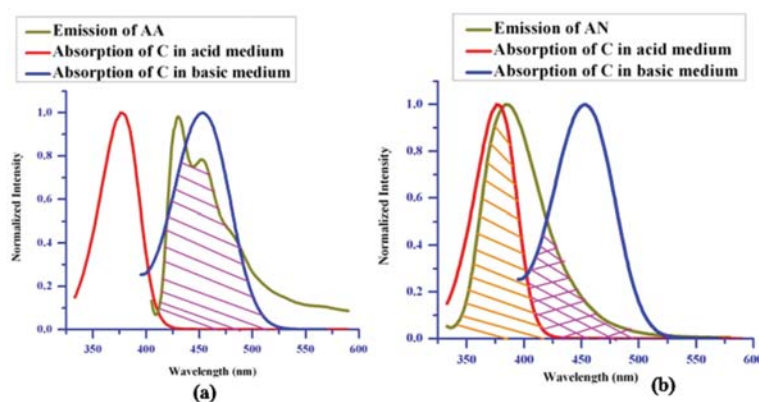


Fig. 2 Overlap between the donor emission and acceptor absorbance for the FRET process of (a) AAC and (b) ANC. The red and blue lines show the normalized absorption of C at acidic and basic pH, respectively. The light green line shows the normalized emission spectra of (a) AA and (b) AN.

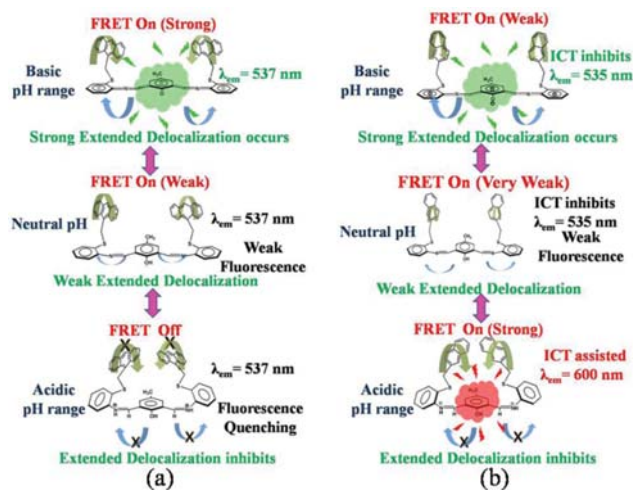


Fig. 3 A plausible mechanism for the emission properties of (a) AAC and (b) ANC.

absorption spectrum of the C unit at acidic pH to a greater extent than at basic or neutral pH. Hence, a stronger “FRET ON” is observed at acidic pH. Moreover, protonation of both of the imine nitrogens causes a loss of planarity and brings the naphthalene moieties closer to the C unit (this is also supported by DFT studies). In addition, an accumulation of positive charge at the nitrogen centers makes intra-molecular charge transfer (ICT) easier, illustrated by the appearance of a new charge transfer absorption band at 525 nm and a substantial red shift of the emission band from 535 nm to 600 nm. Furthermore, an overlap of the emission spectrum of the AN unit with the absorption band of the C unit at acidic pH makes the FRET process feasible and, therefore, an enhancement of the emission intensity at 600 nm in the acidic pH range is due to the ICT-assisted FRET process.

Like AAC, at basic pH, ANC becomes more planar with an extended delocalization of the lone pair of the phenoxide ion, which enhances the emission intensity at 535 nm (Fig. 3b). Although this extended delocalization is absent at acidic pH, a larger emission–absorption overlap and a shorter inter-

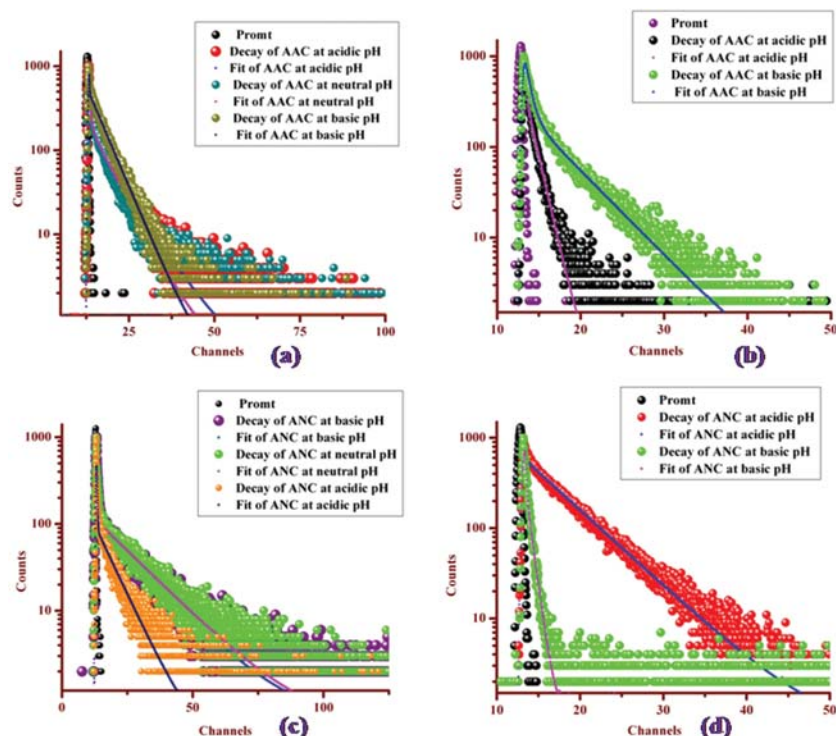


Fig. 4 Fluorescence lifetime decay study of (a) AAC, $\lambda_{\text{em}} = 460$ nm; (b) AAC, $\lambda_{\text{em}} = 537$ nm; (c) ANC, $\lambda_{\text{em}} = 400$ nm; and (d) ANC, $\lambda_{\text{em}} = 600$ nm at pH 2.0 and $\lambda_{\text{em}} = 535$ nm at pH 11.0.

chromophore distance²² make the FRET process stronger (Fig. 2b and 3b). The weak emission intensity of ANC at neutral pH may be attributed to the weak extended delocalization of the lone pair of the phenolic OH group and the relatively high interchromophore distance compared to that seen at an acidic pH. In order to characterize the FRET mechanism, the donor and acceptor have been investigated individually by studying the monochromophoric model compounds; AAP, ANP and APC). By replacing the acceptor C unit with a pyridine moiety, two new model compounds, AAP and ANP, were prepared (Scheme 2). Meanwhile, replacing the donor (either anthracene or naphthalene) unit with the same pyridine moiety, another model compound, APC was also prepared (Scheme 1). AAP and ANP do not show any significant fluorescence changes with variation of pH (Fig. S28 and S29, ESI[†]). However, APC shows a fluorescence enhancement at basic pH due to extended delocalization (Fig. S30, ESI[†]). However, the extent of the fluorescence enhancement is much less than that observed for either AAC or ANC. Negligible changes in the emission intensity for all the

three model compounds (APC, AAP and ANP) at acidic pH strongly suggests the absence of a FRET processes in these monochromophoric compounds.

Fluorescence lifetime decay and DFT studies (see ESI[†]) further support the presence of a FRET process in AAC and ANC. The pK_a values of AAC and ANC have been calculated from fluorescence experiments and are discussed in detail in the ESI.[†] The two pK_a values for AAC are 6.2 ± 0.1 (for pK_{a1} at acidic pH, Fig. S31, ESI[†]) and 8.2 ± 0.1 (for pK_{a2} at basic pH, Fig. S32, ESI[†]). While for ANC, the values are 5.8 ± 0.1 (for pK_{a1} at acidic pH, Fig. S33, ESI[†]) and 8.3 ± 0.1 (for pK_{a2} at basic pH, Fig. S34, ESI[†]). These pK_a values indicate that the color change occurs within the vicinity of neutral pH, which is useful for intracellular studies. The pK_a values of AAC and ANC were calculated from the fluorescence experiments.

3.3 Fluorescence life-time decay studies

The average donor lifetime in AAC ($\lambda_{\text{em}} = 460$ nm) is 0.06 ns (Fig. 4a) at pH 12.0, which increases as the pH changes from

Table 1

	Donor lifetime (AA or AN)		Acceptor (C unit) lifetime	
AAC	pH 4.0 ($\lambda_{\text{em}} = 460$ nm)	4.23 ns	pH 4.0 ($\lambda_{\text{em}} = 537$ nm)	0.05 ns
	pH 7.0 ($\lambda_{\text{em}} = 460$ nm)	2.45 ns	pH 7.0 ($\lambda_{\text{em}} = 537$ nm)	0.32 ns
	pH 12.0 ($\lambda_{\text{em}} = 460$ nm)	0.06 ns	pH 12.0 ($\lambda_{\text{em}} = 537$ nm)	1.35 ns
ANC	pH 2.0 ($\lambda_{\text{em}} = 400$ nm)	0.64 ns	pH 2.0 ($\lambda_{\text{em}} = 600$ nm)	0.20 ns
	pH 7.0 ($\lambda_{\text{em}} = 400$ nm)	6.57 ns	pH 7.0 ($\lambda_{\text{em}} = 535$ nm)	0.03 ns
	pH 12.0 ($\lambda_{\text{em}} = 400$ nm)	1.23 ns	pH 12.0 ($\lambda_{\text{em}} = 535$ nm)	0.07 ns

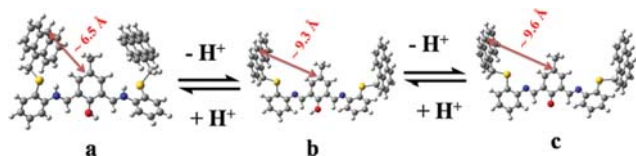


Fig. 5 The optimized geometry of AAC in its protonated (a), neutral (b) and deprotonated (c) forms along with the corresponding donor–acceptor distances.

neutral (pH 7.0) to acidic (pH 4.0), having values of 2.45 ns and 4.23 ns, respectively. In contrast, average acceptor lifetime in AAC ($\lambda_{Em} = 537$ nm) at pH 12.0 is 1.35 ns, significantly longer than its value (0.05 ns) at pH 4.0 (Fig. 4b). Likewise, the average donor lifetime in ANC ($\lambda_{Em} = 400$ nm) at neutral pH is 6.57 ns, which is reduced (by almost 5 times) at pH = 12.0 to 1.23 ns and is further reduced (by almost 10 times) at pH 2.0 to 0.64 ns (Fig. 4c). The average acceptor lifetime in ANC at acidic pH ($\lambda_{Em} = 600$ nm) is 0.20 ns, whereas it is 0.07 ns in basic pH ($\lambda_{Em} = 535$ nm, Fig. 4d) (*vide supra*). All of the results are presented in Table 1.

3.4 Computational studies

Fig. 5 clearly shows that the distance between anthracene and C unit in AAC is less at acidic pH (a) compared to its other forms (b and c). A similar observation is found in ANC (Fig. 6). The theoretical UV-Vis spectrum of the protonated AAC shows predominant transitions (due to the AA unit) at 394, 414 and 435 nm, which are assigned to HOMO – 5 \rightarrow LUMO + 1, HOMO – 1 \rightarrow LUMO + 3 and HOMO – 6 \rightarrow LUMO, respectively. On the other hand, the deprotonated form of AAC shows a dominant transition (due to the C unit) at 504 nm, which is attributed to HOMO \rightarrow LUMO + 2 (Fig. 7).

Moreover, two theoretical peaks (from the TDDFT studies) of protonated ANC at 532 nm (HOMO – 1 \rightarrow LUMO + 1) and 527 nm (HOMO \rightarrow LUMO + 1) are in close agreement with the experimental intra-molecular CT band at 525 nm (Fig. S8, ESI[†]). As indicated in Fig. 8, the electron densities of the HOMO and HOMO – 1 reside on the naphthalene unit, whereas the electron density of LUMO + 1 resides on the AC unit. The deprotonated form of ANC shows two theoretical peaks at 365 nm and 437 nm, which are close to the experimental peaks at 355 nm and 406 nm assigned to HOMO – 4 \rightarrow LUMO and HOMO \rightarrow LUMO transitions, respectively. In both cases, the charge densities of the HOMO – 4 and HOMO are localized predominantly on the C unit, whereas the

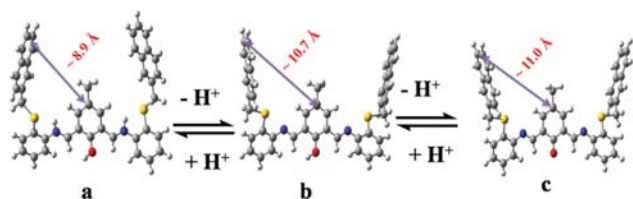


Fig. 6 The optimized geometry of ANC in its protonated (a), neutral (b) and deprotonated (c) forms along with the corresponding donor–acceptor distances.

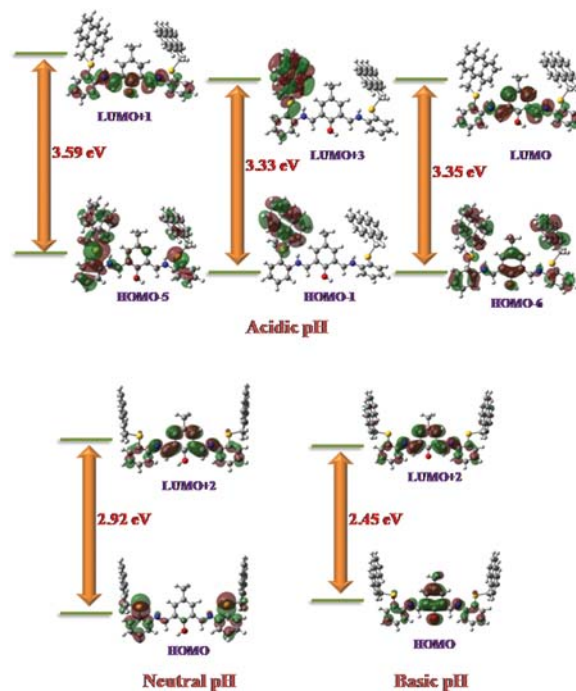


Fig. 7 Charge density distribution of different HOMOs and LUMOs, along with the respective energy gaps for AAC at acidic, neutral and basic pH.

electron density of the LUMO is greater on the AC unit, indicating an extended delocalization.

3.5 Cell imaging studies

Pollen grains are single cells with different pH environments. In the presence of AAC, the pollen grain turns green indicating a

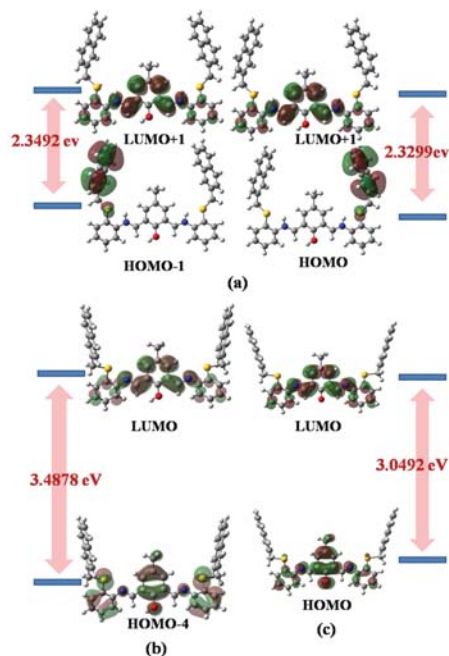


Fig. 8 Charge density distribution in different HOMOs and LUMOs along with the respective energy gaps for ANC at (a) acidic, (b) neutral and (c) basic pH.

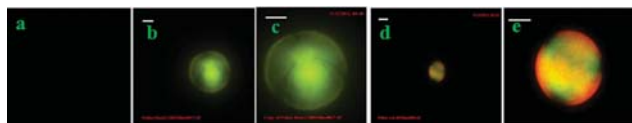


Fig. 9 Cell imaging studies showing (a) blank cell, (b) cell treated with AAC, (c) enlarged view of the cell in (b), (d) cell treated with ANC and (e) enlarged view of the cell in (d). The white scale bar is 10 μ m.

basic pH (Fig. 9b and 9c). Interestingly, ANC can be used to illuminate different parts of the cell showing red and green colors, which indicates that there are different pH environments inside the living cell (Fig. 9d and 9e). Cell viability studies (Fig. S35, ESI[†]) indicate that 90% of the cells remain alive in the presence of the probe even after three days.

4. Conclusion

The facile synthesis of two novel fluorescent probes, AAC and ANC, has been reported. AAC emits green light at basic pH, but is colorless at acidic pH. On the other hand, ANC emits red light at acidic pH, green light at basic pH, but is colorless at neutral pH. The color changes of the sensors can be attributed to the combined effect of extended delocalization and a FRET process. The different behaviour of AAC and ANC at acidic pH has been rationalized on the basis of an intra-molecular charge transfer and enhanced FRET efficiency. ANC can be used to distinguish different pH environments allowing the monitoring of pH within a living cell for the first time.

Acknowledgements

Arnab Banerjee, Animesh Sahana and Sisir Lohar are grateful to CSIR, New Delhi for a fellowship. Sincere thanks to the Indian Institute of Chemical Biology (IICB), Kolkata for extending NMR and mass spectrometer facilities. Special thanks to the University Science Instrumentation Center (USIC), Burdwan University, for providing the fluorescence microscope facility. We are grateful to Prof. Asok Kumar Mukherjee for his helpful discussion and inspiration. The authors sincerely thank Prof. Samita Basu and Mr Ajay Das, Chemical Science Division, SINP, Kolkata for extending TCSPC instrument facility.

Notes and references

- 1 A. Roos and W. F. Boron, *Physiol. Rev.*, 1981, **61**, 296.
- 2 A. Kotyk and J. Slavik, *Intracellular pH and its Measurement*, CRC Press, Boca Raton, FL, 1989
- 3 D. Perez-Sala, D. Collado-Escobar and F. Mollinedo, *J. Biol. Chem.*, 1995, **270**, 6235.
- 4 R. A. Gottlieb, J. Nordberg, E. Skowronski and B. M. Babior, *Proc. Natl. Acad. Sci. U. S. A.*, 1996, **93**, 654.
- 5 S. Simon, D. Roy and M. Schindler, *Proc. Natl. Acad. Sci. U. S. A.*, 1994, **91**, 1128.
- 6 A. Varadiand and G. A. Rutter, *Endocrinology*, 2004, **145**, 4540.
- 7 E. Liang, P. Liu and S. Dinh, *Int. J. Pharm.*, 2007, **338**, 104.
- 8 (a) H. Zhao, X. Xu, J. Diaz and S. Muallem, *J. Biol. Chem.*, 1995, **270**, 19599; (b) I. Yuliand and A. Oplatka, *Science*, 1987, **235**, 340; (c) A. J. Janecki, M. H. Montrose, P. Zimniak, A. Zweibaum, C. M. Tse, S. Khurana and M. Donowitz, *J. Biol. Chem.*, 1998, **273**, 8790.
- 9 A. J. Bullock, R. A. Duquette, N. Buttell and S. Wray, *Pflugers Arch.*, 1998, **435**, 575.
- 10 H. Izumi, T. Torigoe, H. Ishiguchi, H. Uramoto, Y. Yoshida, M. Tanabe, T. Ise, T. Murakami, T. Yoshida, M. Nomoto and K. Kohno, *Cancer Treat. Rev.*, 2003, **29**, 541.
- 11 T. A. Davies, R. E. Fine, R. J. Johnson, C. A. Levesque, W. H. Rathbun, K. F. Seetoo, S. J. Smith, G. Strohmeier and L. Volicer, *et al.*, *Biochem. Biophys. Res. Commun.*, 1993, **194**, 537.
- 12 M. Schindler, S. Grabski, E. Hoff and S. Simon, *Biochemistry*, 1996, **35**, 2811.
- 13 Y. Mathieu, J. Guern, A. Kurkdjian, P. Manigault, J. Manigault, T. Zielinska, B. Gillet, J. C. Beloeil and J. Y. Lallemand, *Plant Physiol.*, 1988, **89**, 19.
- 14 S. Ohkuma and B. Poole, *Proc. Natl. Acad. Sci. U. S. A.*, 1978, **75**, 3327.
- 15 A. Abiko and S. Masamune, *Tetrahedron Lett.*, 1996, **37**, 1081.
- 16 A. E. Ashford and R. B. Knox, *Cell Sri.*, 1980, **44**, 1.
- 17 N. P. Matveeva, D. S. Andreyuk, O. O. Voitsekh and I. P. Ermakov, *Russ. J. Plant Physiol.*, 2003, **50**, 318.
- 18 (a) J. Han and K. Burgess, *Chem. Rev.*, 2010, **110**, 2709; (b) R. Wang, C. Yu, F. Yu and L. Chen, *TrAC, Trends Anal. Chem.*, 2010, **29**, 1004; (c) J. Han, A. Loudet, R. Barhoumi, R. C. Burghardt and K. Burgess, *J. Am. Chem. Soc.*, 2009, **131**, 1642; (d) S. Chen, J. Liu, Y. Liu, H. Su, Y. Hong, C. K. W. Jim, R. T. K. Kwok, N. Zhao, W. Qin, J. W. Y. Lam, K. S. Wong and B. Z. Tang, *Chem. Sci.*, 2012, **3**, 1804.
- 19 (a) A. Banerjee, A. Sahana, S. Guha, S. Lohar, I. Hauli, S. K. Mukhopadhyay, J. S. Matalobos and D. Das, *Inorg. Chem.*, 2012, **51**, 5699; (b) A. Banerjee, A. Sahana, S. Das, S. Lohar, S. Guha, B. Sarkar, S. K. Mukhopadhyay, A. K. Mukherjee and D. Das, *Analyst*, 2012, **137**, 2166; (c) A. Banerjee, D. Karak, A. Sahana, S. Guha, S. Lohar and D. Das, *J. Hazard. Mater.*, 2011, **186**, 738; (d) A. Sahana, A. Banerjee, S. Das, S. Lohar, D. Karak, B. Sarkar, S. K. Mukhopadhyay, A. K. Mukherjee and D. Das, *Org. Biomol. Chem.*, 2011, **9**, 5523; (e) A. Sahana, A. Banerjee, S. Guha, S. Lohar, A. Chattopadhyay, S. K. Mukhopadhyay and D. Das, *Analyst*, 2012, **137**, 1544; (f) S. Das, S. Guha, A. Banerjee, S. Lohar, A. Sahana and D. Das, *Org. Biomol. Chem.*, 2011, **9**, 7097; (g) S. Guha, S. Lohar, A. Banerjee, A. Sahana, A. Chatterjee, S. K. Mukherjee, J. S. Matalobos and D. Das, *Talanta*, 2012, **91**, 18; (h) A. Sahana, A. Banerjee, S. Lohar, S. Guha, S. Das, S. K. Mukhopadhyay and D. Das, *Analyst*, 2012, **137**, 3910; (i) A. Banerjee, A. Sahana, S. Lohar, I. Hauli, S. K. Mukhopadhyay, D. A. Safin, M. G. Babashkina, M. Bolte, Y. Garcia and D. Das, *Chem. Commun.*, 2013, **49**, 2527–2529; (j) S. Lohar, A. Sahana, A. Banerjee, A. Banik, S. K. Mukhopadhyay, J. S. Matalobos and D. Das, *Anal. Chem.*, 2013, **85**, 1778; (k) A. Sahana, A. Banerjee, S. Lohar, B. Sarkar, S. K. Mukhopadhyay and D. Das, *Inorg. Chem.*, 2013, **52**, 3627.

- 20 (a) M. Royzen, Z. Dai and J. W. Canary, *J. Am. Chem. Soc.*, 2005, **127**, 1612; (b) A. Ajayaghosh, P. Carol and S. Sreejith, *J. Am. Chem. Soc.*, 2005, **127**, 14962; (c) K. Kiyose, H. Kojima, Y. Urano and T. Nagano, *J. Am. Chem. Soc.*, 2006, **128**, 6548; (d) S. Banthia and A. Samanta, *J. Phys. Chem. B*, 2006, **110**, 6437; (e) J. R. Lakowicz, *Principles of Fluorescence Spectroscopy*, 3rd edn, Springer, New York, 2008.
- 21 (a) M. Mukhopadhyay, D. Banerjee and S. Mukherjee, *J. Phys. Chem. A*, 2006, **110**, 12743; (b) S. Mitra and S. Mukherjee, *J. Lumin.*, 2006, **118**, 1.
- 22 (a) J. R. Lakowicz, *Principles of Fluorescence Spectroscopy*, 2nd edn, 1999, Ch. 13; (b) A. Albini, E. Fasani and D. Faiardi, *J. Org. Chem.*, 1987, **52**, 155.
- 23 (a) S. Miertus, E. Scrocco and J. Tomasi, *Chem. Phys.*, 1981, **55**, 117; (b) M. Cossi, V. Barone, R. Cammi and J. Tomasi, *Chem. Phys. Lett.*, 1996, **255**, 327; (c) M. Cossi, V. Barone and M. A. J. Robb, *Chem. Phys.*, 1999, **111**, 5295; (d) M. Cossi, G. Scalmani, N. Rega and V. J. Barone, *Chem. Phys.*, 2002, **117**, 43.